Available online at www.sciencedirect.com
SCIENCE DIRECT®
Journal of Power Sources 123 (2003) 26–36
JOURNAL OF POWER SOURCES
www.elsevier.com/locate/jpowsour

Mechanistic approach to performance equations for cathodes in polymer electrolyte fuel cells

Hsiao-Kuo Hsuen [a,b,*]

[a] *Department of Chemical Engineering, Yuan-Ze University, Chung-Li 320, Taiwan, ROC*
[b] *Fuel Cell Center, Yuan-Ze University, Chung-Li 320, Taiwan, ROC*

Received 13 February 2003; accepted 18 March 2003

Abstract

Performance equations that describe the dependence of cathode potential on current density for polymer electrolyte fuel cells (PEFCs) are developed based on a mechanistic approach. The equations take into account, in detail, potential losses caused by: (i) electric resistance and gas transport limitations in the gas diffuser; (ii) limitations of oxygen diffusion, proton migration and electron conduction in the catalyst layer; (iii) oxygen reduction within the catalyst layer. Derivation of the equations is initiated with the formulation of a one-dimensional model and followed by the incorporation of appropriate profiles for oxygen concentration, ionomer potential and catalyst potential. The final forms of the equations are obtained by lumping the oxygen reduction reaction at a reaction center of the catalyst layer. Since the equations are derived from a mechanistic model, all parameters appearing in the equations are endowed with a precise physical meaning. In addition, potential losses caused by various sources can be clearly quantified. Excellent agreement is found between the results obtained from the equations and from the one-dimensional model over an extensive range of the values of model parameters. This indicates that the present equations can be employed to replace the one-dimensional model as an efficient and convenient predictive tool for cathode performance with greatly reduced computational efforts while keeping the same level of accuracy.
© 2003 Elsevier Science B.V. All rights reserved.

Keywords: Fuel cell; Polymer electrolyte; Performance equation; Mechanistic approach

1. Introduction

Due to their promising application as a power generation device in electric vehicles, polymer electrolyte fuel cells (PEFCs) have received increasing attention during the past decade. Parallel to the enhancements in the efficiency and stability of PEFCs by the development of improved components and fabrication techniques, progress in mathematical modelling has provided a deeper insight into the physical and chemical processes as an aid to better design and appropriate operation.

Mathematical models with varying degrees of sophistication in transport phenomena and spatial dimensionality have been developed. Rigorous formulation of a complete cell with the membrane-electrode-assembly and the gas flow channels leads to a three-dimensional model [1,2]. In addition to oxygen transport normal to the gas-diffuser face, different considerations arise with a two-dimensional design, such as variation in oxygen concentration along the gas channels [3–6], inaccessibility on the face of the gas diffuser to oxygen gases due to the rib structure of carbon plates [7–9], or interdigitated flow fields [10]. With different assumptions, wide variations can also be found in the one-dimensional PEFC models [11–18]. Without taking spatial gradients of concentration and potential into account, PEFC models in the form of algebraic equations have also been proposed [19–24].

Based on the methodologies in formulation, the PEFC models can be considered as mechanistic, empirical, or semi-empirical in nature. A mechanistic model is derived from phenomenological mass transport and conservation equations. Thus, the complexity of the models varies with the mechanisms taken into account. On the other hand, an empirical model is typically one equation composed of a few terms that account for the observed characteristics of experimental data. A semi-empirical model is featured by the characteristics of both approaches. A complex mechanistic model is formulated in a more involved way and thus it is able not only to exhibit a great predictive power but to provide a better interpretation of experimental data as well. In addition to the considerable modelling and computational efforts that are required, the model parameters governing

* Tel.: +886-3-463-8800x569; fax: +886-3-455-9373.
E-mail address: skhsun@ce.yzu.edu.tw (H.-K. Hsuen).

0378-7753/$ – see front matter © 2003 Elsevier Science B.V. All rights reserved.
doi:10.1016/S0378-7753(03)00511-1

Nomenclature

a	parameter in Eq. (24)
A	effective platinum surface area per unit volume ($cm^2\,cm^{-3}$)
c_{O_2}	oxygen concentration ($mol\,cm^{-3}$)
$c_{O_2,ref}$	reference oxygen concentration ($mol\,cm^{-3}$), defined as P/H_{O_2}
d	gas-diffuser thickness (mm)
D^{eff}_{i-j}	effective binary diffusion coefficient for i and j species ($cm^2\,s^{-1}$)
$D^{eff}_{O_2}$	effective diffusivity of dissolved oxygen in the catalyst layer ($cm^2\,s^{-1}$)
F	Faraday's constant (96,487 C per equivalent)
H_{O_2}	Henry's constant for oxygen ($atm\,cm^3\,mol^{-1}$)
i	protonic current density ($A\,cm^{-2}$)
i_e	electronic current density ($A\,cm^{-2}$)
$i_{o,ref}$	exchange current density at reference condition ($A\,cm^{-2}$)
I	cathode current density ($A\,cm^{-2}$)
I_o	reference current density ($A\,cm^{-2}$), defined by Eq. (11f)
k^{eff}_d	effective electronic conductivity for gas diffuser ($mho\,cm^{-1}$)
k^{eff}_m	effective protonic conductivity for the ionomer phase ($mho\,cm^{-1}$)
k^{eff}_s	effective electronic conductivity for solid catalysts ($mho\,cm^{-1}$)
n	number of electrons transferred in reaction
N_i	molar flux of species i ($mol\,cm^{-2}$)
P	total pressure (atm)
R	the universal gas constant ($8.314\,J\,mol^{-1}\,K^{-1}$)
T	cathode temperature (K)
V	potential of catalysts (V)
V^*	catalyst potential at reaction center (V)
V_c	cathode potential (V)
V_o	equilibrium potential (V)
w	dimensionless position where oxygen depletion occurs
x_i	molar fraction of species i
$\bar{x}_{O_2}$	average value of x_{O_2} over catalyst layer
$x^s_{O_2}$	x_{O_2} at catalyst-layer|gas-diffuser interface
z	co-ordinate perpendicular to face of the gas diffuser (μm)

Greek letters

α_i	electrode transfer coefficient
β_i	parameter, defined by Eq. (11b) ($mho\,cm^{-2}$)
β_2	parameter, defined by Eq. (11c) ($mho\,cm^{-2}$)
β_3	parameter, defined by Eq. (28) ($mho\,cm^{-2}$)
β_4	parameter, defined by Eq. (33) ($A^{-1}\,cm^2$)
γ	kinetic coefficient taken as unity
δ	the catalyst-layer thickness (μm)
ζ	dimensionless co-ordinate, defined by Eq. (11d)
ϕ	ionomer potential (V)
ϕ^*	ionomer potential at the reaction center (V)
φ	parameter, defined by Eq. (11a)

the various sources of polarization within the PEFCs are related in a complex nature that cannot be easily captured. In other respects, empirical models are characterized by a simple algebraic expression that relates cell potential and current density [19–21]. Due to the lack of physical origin and significance in the model parameters, however, they are abundant with fitting coefficient which thus eliminates the possibility of using them as predictive tools. In order to circumvent the drawbacks of empirical models, semi-empirical formulation of a performance equation has been proposed to reduce the number of fitting coefficients, in which both mechanistic and empirical features are present in the model parameters [22–25].

In the present work, an attempt is made to derive performance equations with all mechanistic derived coefficients. In order to do this, attention is first paid to the chemical and transport phenomena that occur in the cathode of a PEFC and formulate a one-dimensional mechanistic model that takes into account spatial variations of concentration and potential in the catalyst layer and the gas diffuser. By approximating the concentration and potential profiles with appropriate shape functions and lumping the oxygen reduction reaction at the reaction center, it is possible to reduce the one-dimensional model to a single performance equation that presents the relationship between cathode potential and current density. Because the performance equations are derived from a mechanistic model, they can be employed as a predictive tool while characterized by simple algebraic expression just like empirical model equations. In addition, individual contributive terms to the overall cathode polarization can be clearly identified. Computational results also reveal that excellent agreement exists between the polarization curves (calculated based on the one-dimensional model) and the developed performance equations. This indicates that the derived performance equations can be used as a replacement for the one-dimensional model without introducing any appreciable errors.

2. One-dimensional model

The mathematical model for the PEFC cathodes considered in the present work is a one-dimensional, steady-state and isothermal model. The cathodes are composed of two major components, namely, a catalyst layer and a gas diffuser. In the former, it is assumed that catalyst particles, usually in the form of platinum supported on carbon black or of

unsupported platinum black, are homogeneously mixed with a proton-conductive ionomer. The gas diffuser, which is in intimate contact with the catalyst layer, is made of carbon paper or carbon cloth with hydrophobic treatment. During operation, oxygen gases, mostly coming from a humidified air stream, penetrate the gas diffuser to reach its interface with the catalyst layer, and then dissolve into the ionomer phase. Since the ionomer consists of both hydrophobic branches and hydrophilic groups, there might also exist some void spaces in the catalyst layer. Thus, some oxygen gases will diffuse further into the inner region of the catalyst layer via gas channels, and dissolve into the ionomer phase thereby. In the ionomer phase, the dissolved oxygen will continue to travel to the surface of the platinum particles, where an electrochemical reaction with the protons from the anode occurs and can be described by

$$4H^+ + 4e^- + O_2 \Leftrightarrow 2H_2O$$

The Bulter–Volmer equation for the rate of the above electrochemical reaction gives

$$\nabla \cdot i = A i_{o,\mathrm{ref}} \left(\frac{c_{O_2}}{c_{O_2,\mathrm{ref}}}\right)^{\gamma} \left[\exp\left(\frac{-\alpha_a nF(V_o - V + \phi)}{RT}\right) - \exp\left(\frac{\alpha_c nF(V_o - V + \phi)}{RT}\right)\right] \quad (1)$$

where α_i is the electrode transfer coefficient; i the protonic current density; A the effective platinum surface area per unit volume; $i_{o,\mathrm{ref}}$ is the exchange current density at the reference condition; γ a kinetic coefficient and taken as unity; T the temperature of the catalyst layer; R the universal gas constant; c_{O_2} the dissolved oxygen concentration; n the number of electrons transferred in the reaction; V_o the equilibrium potential; V the catalyst potential; and ϕ the ionomer potential.

The mass-balance equation of oxygen in the catalyst layer can be written as

$$D_{O_2}^{\mathrm{eff}} \nabla^2 c_{O_2} + \frac{\nabla \cdot i}{nF} = 0 \quad (2)$$

in which $D_{O_2}^{\mathrm{eff}}$ is the effective diffusivity of dissolved oxygen in the catalyst layer. As stated previously, oxygen may diffuse in the catalyst layer via different paths, i.e. gas pores or hydrated ionomer. In fact, the value of $D_{O_2}^{\mathrm{eff}}$ may vary significantly due to the various degrees of involvement of these two different diffusion routes. In the present study, the details of the oxygen diffusion mechanism are not considered. Instead, $D_{O_2}^{\mathrm{eff}}$ is treated as an adjustable parameter so as to investigate its influence on cathode performance and to explore the discrepancies between the performance equations and the one-dimensional model under different rates of oxygen transport. The ohmic potential losses in the catalyst layer are attributed to both proton migration through the ionomer phase and electron conduction in the solid catalysts. Applying Ohm's law to the motion of both the proton and the electrons gives

$$\frac{dV}{dz} = \frac{i_e}{k_s^{\mathrm{eff}}} \quad (3)$$

and

$$\frac{d\phi}{dz} = -\frac{i}{k_m^{\mathrm{eff}}} \quad (4)$$

where k_s^{eff} and k_m^{eff} denote the effective electric conductivity for the solid catalysts and the effective protonic conductivity for the ionomer phase, respectively, and i_e represents the electronic current density. From electroneutrality, one obtains

$$\nabla \cdot i + \nabla \cdot i_e = 0 \quad (5)$$

As a humidified air stream is used as the cathode feed, three gaseous species, viz. oxygen, nitrogen and water vapor, exist in the diffusion layer. The Stefan–Maxwell equations for multi-component diffusion are usually a starting point for the description of gas transport in the gas diffuser, and take the form

$$\nabla x_i = \sum_{j=1}^{n} \frac{RT}{PD_{i-j}^{\mathrm{eff}}} (x_i N_j - x_j N_i), \quad i = N_2, w, O_2 \quad (6)$$

where D_{i-j}^{eff} is an effective binary diffusion coefficient in the porous medium for i and j species and N_i the molar flux of species i with x_i its molar fraction. It is assumed that a phase equilibrium between the water vapor and its condensed phase is achieved at each point of the gas diffuser. Also, the molar flux of nitrogen is taken to be zero due to its inertness. Thus, the Stefan–Maxwell equations can be condensed into one single equation [13], i.e.

$$\frac{P}{RT}\nabla x_{O_2} = -(1 - x_w - x_{O_2}) N_{O_2} \times \left[\frac{1}{D_{N_2-O_2}^{\mathrm{eff}}} + \frac{x_w}{x_{O_2} D_{N_2-w}^{\mathrm{eff}} + (1 - x_w - x_{O_2}) D_{O_2-w}^{\mathrm{eff}}}\right] \quad (7)$$

In order to facilitate computations, the above equations were rearranged and written in partially dimensionless form. In the catalyst layer ($0 < \zeta < 1$)

$$\frac{d^2 x_{O_2}}{d\zeta^2} - \varphi \left[\exp\left(\frac{\alpha_c nF(V_0 - V + \phi)}{RT}\right) - \exp\left(\frac{-\alpha_a nF(V_0 - V + \phi)}{RT}\right)\right] x_{O_2} = 0 \quad (8)$$

$$\frac{\beta_1}{I_o}\frac{d^2 V}{d\zeta^2} + \frac{d^2 x_{O_2}}{d\zeta^2} = 0 \quad (9)$$

$$\frac{d^2 x_{O_2}}{d\zeta^2} - \frac{\beta_2}{I_o}\frac{d^2 \phi}{d\zeta^2} = 0 \quad (10)$$

where

$$\varphi = \frac{Ai_{o,ref} H_{O_2} \delta^2}{nFPD_{O_2}^{eff}} \tag{11a}$$

$$\beta_1 = \frac{k_s^{eff}}{\delta} \tag{11b}$$

$$\beta_2 = \frac{k_m^{eff}}{\delta} \tag{11c}$$

$$\zeta = \frac{z}{\delta} \tag{11d}$$

$$x_{O_2} = \frac{H_{O_2} c_{O_2}}{P} \tag{11e}$$

$$I_o = \frac{nFPD_{O_2}^{eff}}{H_{O_2}\delta} \tag{11f}$$

where δ denotes the catalyst-layer thickness and H_{O_2} the Henry's constant for gaseous oxygen and its dissolved form in the ionomer phase at the cathode temperature. It should be noted that x_{O_2} denotes the molar fraction of oxygen in the gas phase of the diffuser but stands for the dimensionless concentration of dissolved oxygen in the ionomer phase within the catalyst layer as defined by Eq. (11e). The same notation is used in these two domains because by such definitions x_{O_2} profiles are continuous across their boundary.

In the gas diffuser ($1 < \zeta < b$), two more equations are required in addition to Eq. (7), viz.

$$\frac{dN_{O_2}}{d\zeta} = 0 \tag{12}$$

$$\frac{d^2V}{d\zeta^2} = 0 \tag{13}$$

where V is the potential of the carbon paper (or cloth). This is the same symbol as that used for the potential of solid catalysts in the catalyst layer since these two quantities are identical at the boundary between these two regions. At the face of the gas diffuser ($\zeta = b$), two more boundary conditions are required apart from Eq. (12) i.e.

$$x_{O_2} = x_{O_2}^b \tag{14}$$

$$V = V_c \tag{15}$$

where $x_{O_2}^b$ indicates the oxygen molar fraction in the bulk flow and V_c is the cathode potential. At the gas-diffuser|catalyst-layer interface, six boundary conditions are needed since there are three state variables in each domain. First, Eq. (12) is also applied. In addition, continuities of V and x_{O_2} require

$$x_{O_2}\,(\text{catalyst layer}) = x_{O_2}\,(\text{gas diffuser}) \tag{16}$$

$$V\,(\text{catalyst layer}) = V\,(\text{gas diffuser}) \tag{17}$$

Equivalence of oxygen molar flux and electric current density on both sides of the boundary leads to

$$k_s^{eff}\frac{dV}{d\zeta}\,(\text{catalyst layer}) = k_d^{eff}\frac{dV}{d\zeta}\,(\text{gas diffuser}) \tag{18}$$

$$\frac{I_o}{nF}\frac{dx_{O_2}}{d\zeta}\,(\text{catalyst layer}) = -N_{O_2} \tag{19}$$

Because protons are not able to penetrate the catalyst-layer|gas-diffuser interface, zero protonic current is expected here, which gives

$$\frac{d\phi}{d\zeta} = 0 \tag{20}$$

At the membrane|catalyst-layer interface ($\zeta = 0$), the boundary conditions are formulated as

$$\phi = 0 \tag{21}$$

$$\frac{dx_{O_2}}{d\zeta} = 0 \tag{22}$$

$$\frac{dV}{d\zeta} = 0 \tag{23}$$

The mathematical model described above was formulated following the lines of Bernardi and Verbrugge [13] as well as Springer et al. [17]. Compared with the work of Bernardi and Verbrugge [13], a membrane is not included and flow of liquid water in the catalyst layer is not taken into account in the present model for the sake of simplification. Finite values of electric conductivity for the solid catalysts and the gas diffuser are considered to account for ohmic potential loss due to electronic movement, which are neglected in the work of Springer et al. [17].

The model equations derived above form a three-point boundary value problem with three state variables in each domain. The method of collocation on finite elements based on cubic B-spline interpolation was employed for the numerical solutions of the model equations [26]. First, the domains of the gas diffuser and the catalyst layer were divided into several sub-intervals, respectively. Because of the moderate non-linearity of the Stefan–Maxwell equations and the mild steepness for the oxygen concentration profiles developed in the gas diffuser, only three sub-intervals with equal sizes were arranged in this domain. Twelve sub-intervals of non-equal sizes were employed in the catalyst-layer domain to account for high non-linearity of the electrochemical rate expression for the Bulter–Volmer equation and soaring oxygen concentration gradients developed at high current densities. In the catalyst-layer domain, the sizes of the sub-intervals were decreased along the ζ-direction by a common ratio of 0.37. Continuities of the first derivatives of all state variables were required at each breakpoint point of sub-intervals except the gas-diffuser|catalyst-layer interface. Two points were collocated in each sub-interval, which thus transforms the model equations into a set of algebraic equations. Newton's method was employed to obtain the numerical solutions of the resulting algebraic equations.

3. Approximate model I for performance equations

It is assumed that the dimensionless oxygen concentration profile in the catalyst layer can be described by a parabolic function, which has the form

$$x_{O_2} = a\zeta^2 + x^s_{O_2} - a \tag{24}$$

where $x^s_{O_2}$ denotes the value of x_{O_2} at the catalyst-layer|gas-diffuser interface. Eq. (24) naturally satisfies the boundary conditions at $\zeta = 0$ and 1. By relating the current density with the flux of dissolved oxygen at the catalyst-layer|gas-diffuser interface, a can be expressed as

$$a = \frac{I}{2I_o} \tag{25}$$

where I stands for the cathode current density. The profiles of ionomer potential and catalyst potential within the catalyst layer can be easily derived from Eqs. (9), (10) and (24) together with their associated boundary conditions, which are

$$V = -\frac{I}{2\beta_1}\zeta^2 + \frac{I}{2\beta_1} + V_c + \frac{I}{\beta_3} \tag{26}$$

$$\phi = \frac{I}{2\beta_2}\zeta^2 - \frac{I}{\beta_2}\zeta \tag{27}$$

where

$$\beta_3 = \frac{k^{eff}_d}{d} \tag{28}$$

k^{eff}_d represents the effective electric conductivity of the gas diffuser and d its thickness. Furthermore, the anodic reaction rate is neglected and the rate of electrochemical reaction occurring in the catalyst layer is lumped at the reaction center, which is defined by

$$\zeta^* = \frac{\int_0^1 \zeta x_{O_2}\,d\zeta}{\int_0^1 x_{O_2}\,d\zeta} = \frac{3(4x^s_{O_2}I_o - I)}{8(3x^s_{O_2}I_o - I)} \tag{29}$$

Based on the two approximations stated above, one can have

$$I = Ai_{o,ref}\delta\left[\exp\left(\frac{\alpha_c nF(V_0 - V^* + \phi^*)}{RT}\right)\right]\bar{x}_{O_2} \tag{30}$$

where V^* and ϕ^*represent the catalyst potential and the ionomer potential at the reaction center, respectively. $\bar{x}_{O_2}$ stands for the average value of x_{O_2} over the catalyst layer, which is calculated by

$$\bar{x}_{O_2} = \int_0^1 x_{O_2}\,d\zeta = x^s_{O_2} - \frac{I}{3I_o} \tag{31}$$

By following the approach of Pisani et al. [25], that is to approximate $D^{eff}_{w-O_2}$ with $D^{eff}_{N_2-w}$, Eq. (7) can be directly solved and $x^s_{O_2}$ can be expressed as

$$x^s_{O_2} = x^b_{O_2} - x^b_{N_2}[\exp(\beta_4 I) - 1] \tag{32}$$

where

$$\beta_4 = \frac{RTd}{nFP}\left[\frac{1}{D^{eff}_{N_2-O_2}} + \frac{x_w}{(1-x_w)D^{eff}_{N_2-w}}\right] \tag{33}$$

After evaluating V^*, ϕ^* and $\bar{x}_{O_2}$in Eq. (30) with Eq. (26) and (27) and then taking logarithms on both sides, one arrives at

$$V_c = V_o - \frac{I}{128\beta_1}\frac{(36x^s_{O_2}I_o - 11I)(12x^s_{O_2}I_o - 5I)}{(3I_o x^s_{O_2} - I)^2} - \frac{I}{\beta_3} - \frac{3I}{128\beta_2}\frac{(4x^s_{O_2}I_o - I)(36x^s_{O_2}I_o - 13I)}{(3x^s_{O_2}I_o - I)^2} - \frac{RT}{\alpha_c nF}\ln\left[\frac{I}{\varphi(x^s_{O_2}I_o - I/3)}\right] \tag{34}$$

The overall potential loss in a PEFC cathode can be viewed as a summation of diffusion overpotential and ohmic overpotential for electron conduction in the gas diffuser, diffusion overpotential and ohmic potential losses for proton migration and electron conduction in the catalyst layer, and activation overpotential for the electrochemical reaction. It is noted that each individual contribution in the cathode potential loss can be clearly quantified in Eq. (34), which are

$$\text{diffusion overpotential in gas diffuser} = \frac{RT}{\alpha_c nF}\ln\left(\frac{x^b_{O_2}}{x^s_{O_2}}\right) \tag{35}$$

$$\text{activation overpotential for electrochemical reaction} = \frac{RT}{\alpha_c nF}\ln\left(\frac{I}{\varphi x^b_{O_2}I_o}\right) \tag{36}$$

$$\text{diffusion overpotential in catalyst layer} = \frac{RT}{\alpha_c nF}\ln\left(\frac{x^s_{O_2}I_o}{x^s_{O_2}I_o - I/3}\right) \tag{37}$$

$$\text{ohmic loss (electronic) in catalyst layer} = \frac{I}{128\beta_1}\frac{(36x^s_{O_2}I_o - 11I)(12x^s_{O_2}I_o - 5I)}{(3x^s_{O_2}I_o - I)^2} \tag{38}$$

$$\text{ohmic loss (protonic) in catalyst layer} = \frac{3I}{128\beta_2}\frac{(4x^s_{O_2}I_o - I)(36x^s_{O_2}I_o - 13I)}{(3x^s_{O_2}I_o - I)^2} \tag{39}$$

$$\text{ohmic loss (electronic) in diffusion layer} = \frac{I}{\beta_3} \tag{40}$$

Eq. (24) is only valid for the condition that x_{O_2}at the membrane|catalyst-layer interface ($\zeta = 0$) is greater than zero, which indicates

$$I \le 2I_o\{x^b_{O_2} - x^b_{N_2}[\exp(\beta_4 I) - 1]\} \tag{41}$$

As the current density exceeds the critical value, Eq. (41) is no longer satisfied and Eq. (34) is not applicable either. Under such a condition, another function is proposed for the dimensionless oxygen concentration profile within the catalyst layer, namely

$$x_{O_2} = x^s_{O_2}\left(\frac{\zeta - w}{1 - w}\right)^2 \quad \text{for } w \le \zeta \le 1 \quad \text{and}$$
$$x_{O_2} = 0 \quad \text{for } 0 \le \zeta \le w \tag{42}$$

where w denotes the dimensionless position in the catalyst layer where oxygen is completely consumed by the electrochemical reaction. Relating the transport rate of dissolved oxygen at the catalyst-layer|gas-diffuser interface to the electric current density of the cathode results in

$$w = 1 - \frac{2x^s_{O_2} I_o}{I} \tag{43}$$

Accordingly,

$$V = -\frac{x^s_{O_2} I_o}{\beta_1}\left(\frac{\zeta - w}{1 - w}\right)^2 + \frac{x^s_{O_2} I_o}{\beta_1} + \frac{I}{\beta_3} + V_c \quad \text{for } w \le \zeta \le 1$$

$$V = \frac{x^s_{O_2} I_o}{\beta_1} + \frac{I}{\beta_3} + V_c \quad \text{for } 0 \le \zeta \le w \tag{44}$$

$$\phi = \frac{x^s_{O_2} I_o}{\beta_2}\frac{1}{(1-w)^2}(\zeta - w)(\zeta + w - 2) - \frac{wI}{\beta_2} \quad \text{for } w \le \zeta \le 1$$

$$\phi = -\frac{I}{\beta_2}\zeta \quad \text{for } 0 \le \zeta \le w \tag{45}$$

$$\zeta^* = 1 - \frac{x^s_{O_2} I_o}{2I} \tag{46}$$

$$\bar{x}_{O_2} = \frac{2(x^s_{O_2})^2 I_o}{3I} \tag{47}$$

Just following the same procedures as those without oxygen depletion, the cathode potential can be related to the electric current density as

$$V_c = V_o - \frac{7x^s_{O_2} I_o}{16\beta_1} + \frac{17}{16}\frac{x^s_{O_2} I_o}{\beta_2} - \frac{I}{\beta_2} - \frac{I}{\beta_3} - \frac{RT}{\alpha_c nF}\ln\left[\frac{3I^2}{2\varphi(x^s_{O_2} I_o)^2}\right] \tag{48}$$

The diffusion overpotential and the electronic ohmic loss of the gas diffuser and the activation overpotential for the electrochemical reaction have the same expressions as those of Eqs. (35), (36) and (40). Other contributive terms have the forms

diffusion overpotential of catalyst layer

$$= \frac{RT}{\alpha_c nF}\ln\left[\frac{3I}{2I_o x^s_{O_2}}\right] \tag{49}$$

$$\text{ohmic loss (electronic) of catalyst layer} = \frac{7x^s_{O_2} I_o}{16\beta_1} \tag{50}$$

$$\text{ohmic loss (protonic) of catalyst layer} = \frac{I}{\beta_2} - \frac{17}{16}\frac{x^s_{O_2} I_o}{\beta_2} \tag{51}$$

4. Approximate model II for performance equations

The performance equations derived previously can be further simplified if the potential profiles of the solid catalysts and the ionomer phase in the catalyst layer are assumed to be piecewise linear rather than parabolic as stated in the approximate model I. Following the postulation that the electrochemical reaction is lumped at the reaction center, the ionomer potential decreases linearly from the membrane|catalyst-layer interface to the reaction center due to an invariant protonic current density. In addition, the ionomer potential profile becomes flat after the reaction center since the protonic current density is essentially zero in this region. On the other hand, the potential profile of the solid catalysts behaves oppositely. It appears as a horizontal line from the membrane|catalyst-layer interface to the reaction center because of the absence of electronic movement in this region and decreases linearly thereafter due to a constant electronic current. Based on these observations, the potential profiles for the solid catalysts and the ionomer can be written as

$$V = \frac{I}{\beta_1}(1 - \zeta) + \frac{I}{\beta_3} + V_c \quad \text{for } \zeta^* \le \zeta \le 1;$$
$$V = \frac{I}{\beta_1}(1 - \zeta^*) + \frac{I}{\beta_3} + V_c \quad \text{for } 0 \le \zeta \le \zeta^* \tag{52}$$

$$\phi = -\frac{I}{\beta_2}\zeta^* \quad \text{for } \zeta^* \le \zeta \le 1;$$
$$\phi = -\frac{I}{\beta_2}\zeta \quad \text{for } 0 \le \zeta \le \zeta^* \tag{53}$$

As a result, the performance equation becomes

$$V_c = V_o - \frac{I}{\beta_1}\frac{12x^s_{O_2} I_o - 5I}{24x^s_{O_2} I_o - 8I} - \frac{I}{\beta_2}\frac{12x^s_{O_2} I_o - 3I}{24x^s_{O_2} I_o - 8I} - \frac{I}{\beta_3} - \frac{RT}{\alpha_c nF}\ln\left[\frac{I}{\varphi(x^s_{O_2} I_o - I/3)}\right] \tag{54}$$

for the condition without oxygen depletion. Accordingly, ohmic losses due to the electron conduction and proton

migration are modified to

ohmic loss (electronic) in catalyst layer

$$= \frac{I}{\beta_1}\frac{12x^{s}_{O_2}I_o - 5I}{24x^{s}_{O_2}I_o - 8I} \quad (55)$$

ohmic loss (protonic) in catalyst layer

$$= \frac{I}{\beta_2}\frac{12x^{s}_{O_2}I_o - 3I}{24x^{s}_{O_2}I_o - 8I} \quad (56)$$

while other contributive terms in the cathode polarization remain the same. As oxygen depletion occurs, the performance equation is changed to

$$V_c = V_o - \frac{x^{s}_{O_2}I_o}{2\beta_1} + \frac{x^{s}_{O_2}I_o}{2\beta_2} - \frac{I}{\beta_2} - \frac{I}{\beta_3} - \frac{RT}{\alpha_c nF}\ln\left[\frac{3I^2}{2\varphi(x^{s}_{O_2}I_o)^2}\right] \quad (57)$$

Thus, the ohmic losses due to electron conduction and proton migration have to be re-evaluated as

$$\text{ohmic loss (electronic) of catalyst layer} = \frac{x^{s}_{O_2}I_o}{2\beta_1} \quad (58)$$

$$\text{ohmic loss (protonic) of catalyst layer} = \frac{I}{\beta_2} - \frac{1}{2}\frac{x^{s}_{O_2}I_o}{\beta_2} \quad (59)$$

The performance equations derived based on the approximate model II appear to have simpler expressions for the ohmic losses pertinent to proton migration and electron conduction in the catalyst layer than those based on the approximate model I, particularly for the condition that oxygen depletion does not yet occur. At low current density, however, such differences would be of little significance compared with other contributive terms of polarization. At high current densities, most dissolved oxygen in the catalyst layer is consumed within a narrow region close to the catalyst-layer|gas-diffuser interface. Consequently, the potential loss caused by proton migration becomes completely dominant in the ohmic losses of the catalyst layer due to much lower values of protonic conductivity and much longer travel distance for protons. As a result, the differences between the performance equations formulated according to these two approximate models are expected to be negligible. These observations imply that the performance equations of the approximate model II are derived using simpler forms of potential profiles for the ionomer phase and the solid catalysts, but most likely with no appreciable degradation of accuracy. Detailed comparisons based on computations will be delineated in the following sections.

5. Results and discussion

The one-dimensional model and the performance equations formulated in the previous sections have been used to construct the polarization curves for PEFC cathodes in order to investigate the accuracy of the performance equations. The parameter values used for the base case are listed in Table 1. In fact, due to the variations in the techniques and in the properties of materials used for fabricating a PEFC cathode, the values of its physical and chemical properties may differ by some orders of magnitude. As mentioned previously, the major objective of the present study is to investigate the accuracy of the performance equations by taking the numerical solutions of the one-dimensional model as exact ones for an extended parameter range. In order to do this, computations were carried out by adjusting the magnitude of a particular parameter in Table 1, while other parameter values remain fixed. The loci of the performance equations as well as the solutions of the one-dimensional model for the base case are shown in Fig. 1. There is rather good agreement among these three curves since they cannot be distinguished except the region near the limiting currents. The differences in the limiting currents calculated based on the performance equations and the one-dimensional model are caused partially by the approximation (Eq. (32)) that is used to evaluate the oxygen concentration at the gas-diffuser|catalyst-layer interface,

Table 1
Values of model parameters for base case

Effective ionic conductivity of ionomer, k_m^{eff} (mho cm^{-1})	1.06×10^{-2}
Effective electric conductivity of catalyst, k_s^{eff} (mho cm^{-1})	0.354
Effective electric conductivity of gas diffuser, k_d^{eff} (mho cm^{-1})	0.5
Effective diffusivity of dissolved oxygen in the catalyst layer, $D_{O_2}^{eff}$	4.2×10^{-7}
Effective gas-pair diffusivity, $D_{O_2-N_2}^{eff}$ ($= \varepsilon^{1.5} D_{O_2-N_2}$) (cm^2 s^{-1})	6.97×10^{-3}
Effective gas-pair diffusivity, $D_{N_2-w}^{eff}$ ($= \varepsilon^{1.5} D_{N_2-w}$) (cm^2 s^{-1})	9.67×10^{-3}
Effective gas-pair diffusivity, $D_{O_2-w}^{eff}$ ($= \varepsilon^{1.5} D_{O_2-w}$) (cm^2 s^{-1})	9.48×10^{-3}
Gas-diffuser thickness, d (μm)	300
Catalyst-layer thickness, δ (μm)	10
Effective porosity of gas diffuser, ε	0.25
Product of platinum surface area and reference exchange current, $Ai_{o,ref}$ (A cm^{-3})	4.1×10^{-4}
Pressure, P (atm)	5
Bulk oxygen molar fraction, $x_{O_2}^b$	0.190
Bulk nitrogen molar fraction, $x_{N_2}^b$	0.716
Molar fraction of water vapor, x_w	0.094
Temperature, T (°C)	80
Henry's constant, H_{O_2} (atm cm^3 mol^{-1})	2.0×10^5
Equilibrium potential, V_o (V)	1.2
Cathodic transfer coefficient, α_c	0.5
Anodic transfer coefficient, α_a	0.5

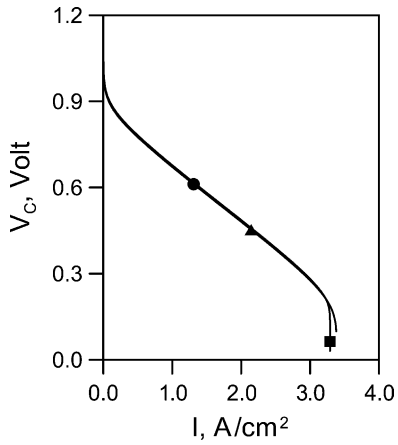

Fig. 1. Polarization curves for base case. (■) One-dimensional model; (▲) approximate model I; (●) approximate model II.

and partially by the numerical errors of the one-dimensional model due to extremely high oxygen concentration gradients developed while the current density approaches its limiting value. The individual contributive terms of the overall cathode polarization for the base case shown in Fig. 1 are displayed in Fig. 2, which are calculated using the performance equations derived from the approximate model II. It is seen that the ohmic potential loss pertinent to electron motion in the catalyst layer is negligible for the entire range of current density because of the high electric conductivity of the solid catalysts and the small thickness of the layer. The activation overpotential for oxygen reduction increases sharply at extremely low current densities. As the current density is further increased, the activation overpotential increases in a more moderate fashion and other contributive terms for the cathode potential losses gain more importance. The potential losses for proton migration in the ionomer

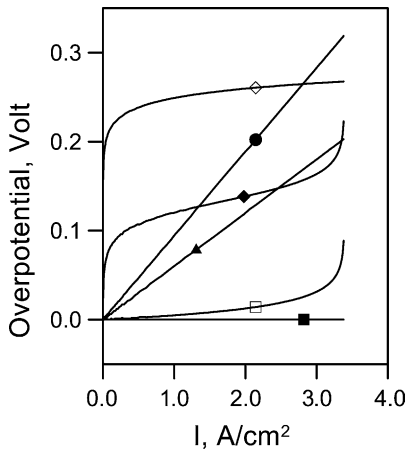

Fig. 2. Polarization curves of individual contributive terms for the base case calculated using approximate model II. (■) Ohmic potential loss of catalyst; (◇) activation overpotential for oxygen reduction reaction; (◆) diffusion overpotential of catalyst layer; (□) diffusion overpotential of gas diffuser; (●) ohmic potential loss of ionomer in catalyst layer; (▲) ohmic potential loss of gas diffuser.

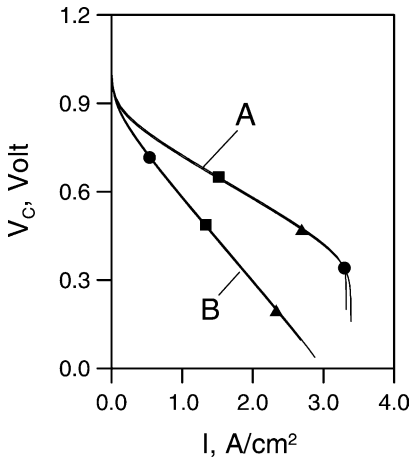

Fig. 3. Polarization curves for cathodes with different catalyst-layer thicknesses. (A) $\delta = 5\,\mu m$; (B) $\delta = 20\,\mu m$; (■) one-dimensional model; (▲) approximate model I; (●) approximate model II.

phase of the catalysts layer and electron conduction in the gas diffuser are quite similar; both appear linear but with different slopes. The diffusion overpotential in the catalyst layer exhibits similar characteristics to those of the activation overpotential at low and intermediate densities; nevertheless, it increases sharply to infinity as the limiting current is approached. Such a phenomenon is also observed for the diffusion overpotential for the gas diffuser due to the vanishing of oxygen concentration at the catalyst-layer|gas-diffuser interface.

The polarization curves for two cathodes with different thickness of the catalyst layer, i.e. 5 and 20 μm, are given in Fig. 3. It is seen that the results calculated based on the performance equations of the approximate models I and II and the one-dimensional model are well matched. At low current densities, oxygen is able to reach every point of the catalyst layer. Thus, a thicker catalyst layer indicates that larger space is available for the oxygen reduction reaction. As a result, a lower activation overpotential is required to generate the same electric current. In other respects, higher values of ohmic potential losses for proton migration is expected for a thicker catalyst layer due to the longer travel distance. Moreover, a higher diffusion overpotential is formed by a lower average value of oxygen concentration over the catalyst layer. Recall that potential loss caused by electron conduction in the catalyst layer is negligible. Computational results reveal that the first factor is more pronounced than the other two at low current densities, which thus results in a higher potential for the cathode with a thicker catalyst layer. At intermediate and high current densities, however, oxygen depletion takes place within the catalyst layer; therefore, the influence of the first factor diminishes and those of the other two become dominant. As a consequence, a higher potential is found for the cathode with a thinner catalyst layer. It should be noted that the diffusion overpotential of the diffuser does not change with the thickness of the catalyst layer as indicated by Eq. (35).

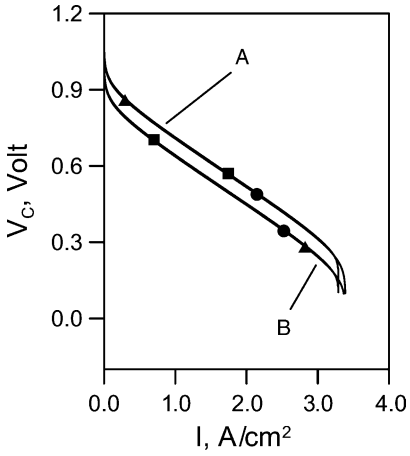

Fig. 4. Polarization curves for cathodes with different product values of $Ai_{o,ref}$. (A) $Ai_{o,ref} = 4.1 \times 10^{-3}$ $A\,cm^{-3}$; (B) $Ai_{o,ref} = 4.1 \times 10^{-5}$ $A\,cm^{-3}$; (■) one-dimensional model; (▲) approximate model I; (●) approximate model II.

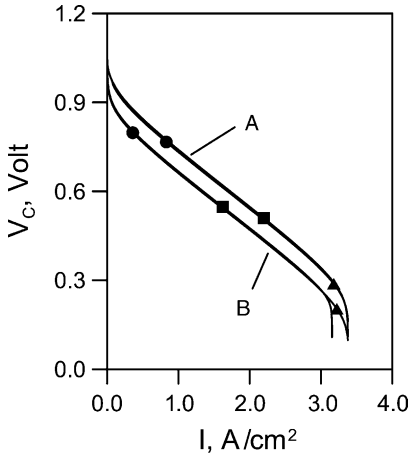

Fig. 5. Polarization curves for cathodes with different values of effective oxygen diffusivity in catalyst layer. (A) $D_{O_2}^{eff} = 2.1 \times 10^{-5}\,cm^2\,s^{-1}$; (B) $D_{O_2}^{eff} = 2.1 \times 10^{-7}\,cm^2\,s^{-1}$; (■) one-dimensional model; (▲) approximate model I; (●) approximate model II.

The polarization curves calculated for two cathodes with different product values of $Ai_{o,ref}$, viz. 4.1×10^{-3} and 4.1×10^{-5} A cm^{-3}, are displayed in Fig. 4. Again, the polarization curves obtained using the approximate models I and II agree well with those from the one-dimensional model. Among all the parameters considered in the present models, $Ai_{o,ref}$ is the only one that characterizes the activity of the cathode catalysts. If $i_{o,ref}$ remains unchanged, a larger product value of $Ai_{o,ref}$ implies that the cathode is composed of catalysts with a higher platinum dispersion, which provide a larger active surface area to accommodate oxygen reduction. For a cathode with a higher value of $Ai_{o,ref}$, a lower activation overpotential is required to generate an identical electric current; thus, a higher cathode potential is expected. Such an effect can be quantitatively estimated by Eq. (36). As shown, a difference of 0.07 V in the cathode potential results from the two different $Ai_{o,ref}$ values used in calculating the results presented in Fig. 4.

Investigation of the discrepancies among the polarization curves from the approximate models I and II and from the one-dimensional model was carried out for cathodes with two different values of effective diffusivity of oxygen in the catalyst layer ($D_{O_2}^{eff}$). The results are presented in Fig. 5. A fairly good agreement is found between the three models as in the previous cases. The parameter $D_{O_2}^{eff}$ provides a quantified measure of the transport ability of oxygen under the multiphase structure of the catalyst layer. A higher value of $D_{O_2}^{eff}$ indicates that oxygen is able to reach a deeper portion of the catalyst layer and, consequently, a lower diffusion overpotential in the catalyst layer results. This, in turn, gives rise to a higher cathode potential. As shown, the difference in limiting current density calculated using the one-dimensional model and the approximate ones for the cathode with $D_{O_2}^{eff} = 2.1 \times 10^{-7}\,cm^2\,s^{-1}$ is much lager than that with $D_{O_2}^{eff} = 2.1 \times 10^{-5}\,cm^2\,s^{-1}$. This is attributed to the fact that a steeper oxygen concentration profile is formed for the catalyst layer with a lower $D_{O_2}^{eff}$, which therefore leads to larger numerical errors in the region near the limiting current. Nevertheless, the present performance equations yield the same values of limiting current for theses two cases.

Polarization curves are constructed in Fig. 6 for two cathodes with different values of effective ionomer conductivity in the catalyst layer by using the three models formulated in the present study. The curves from the three models almost coincide. In addition, the cathode with $k_m^{eff} = 0.035\,mho\,cm^{-1}$ always exhibits a higher cathode potential than that with $k_m^{eff} = 0.0035\,mho\,cm^{-1}$ for the same current density. The computational results also revealed that the effect of k_m^{eff} on the cathode potential is negligible at low current densities and gains more importance as the current density is increased. Although the expression of ohmic potential loss due to proton migration involves exponential

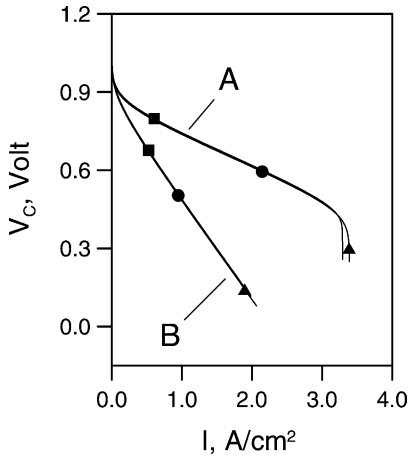

Fig. 6. Polarization curves for cathodes with different values of effective proton conductivity of ionomer phase in catalyst layer. (A) $k_m^{eff} = 0.035$ $mho\,cm^{-1}$; (B) $k_m^{eff} = 0.0035\,mho\,cm^{-1}$; (■) one-dimensional model; (▲) approximate model I; (●) approximate model II.

and fractional functions of current density, it behaves in a linear fashion as illustrated by the results shown in Fig. 2.

The diffusion layer is a very important component in determining the cathode performance at high current densities. Under operation, the effective porosity of the cathode diffuser changes with the amount of liquid water that accumulates in the layer. It depends on the physical and chemical properties of the layer, the degree of external humidification, and the current density. Some research efforts have been made to uncover such dependencies [7,10]. Since the emphasis of the present work is placed on investigating the accuracy of the developed performance equations, a constant value of effective porosity is adopted for the diffuser in calculating the polarization curves. Once an explicit, algebraic expression that describes the reliance of the effective porosity of diffuser on current density and other parameters is available [25], such a relation can be directly incorporated into the present performance equations. The polarization curves for the cathodes with two different ε values are presented in Fig. 7, which have also been calculated using the three models developed in the present work. As illustrated, the polarization curves obtained from the three models are almost identical. At low and intermediate current densities, where the diffusion limitations of oxygen within the diffuser are not significant, the potentials of these two cathodes are quite close. Nevertheless, at high current densities, where the diffusion limitations of oxygen within the diffuser play a more important role in the cathode performance, the cathode with $\varepsilon = 0.1$ yields a lower potential than that with $\varepsilon = 0.4$. As revealed by Eq. (32) and Table 1, variations of ε lead to different values of oxygen concentration at the gas-diffuser|catalyst-layer interface. Thus, except the activation overpotential for oxygen reduction, all other contributive terms to the overall cathode overpotential will, more or less, be influenced by ε. Among these terms, the diffusion overpotential of the diffuser is the one that is most effected. It is also noted that the limiting current density of the cathode with $\varepsilon = 0.1$ is around $0.85\ A\ cm^{-2}$ and the value for the cathode with $\varepsilon = 0.4$ is much higher, which is not covered by the data in Fig. 7.

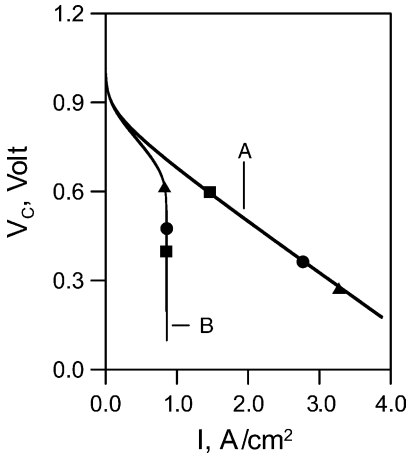

Fig. 7. Polarization curves for cathodes with different effective porosity of gas diffuser. (A) $\varepsilon = 0.4$; (B) $\varepsilon = 0.1$; (■) one-dimensional model; (▲) approximate model I; (●) approximate model II.

6. Summary and conclusions

In the present work, a mechanistic approach has been presented to derive the performance equations for PEFC cathodes. In this approach, the oxygen concentration profile in the catalyst layer is approximated by a parabolic polynomial or a piecewise parabolic relationship, as determined by the occurrence of oxygen depletion. Two different functions, namely, a parabolic and a piecewise linear one, have been suggested to approximate the profiles of the ionomer potential and catalyst potential in the catalyst layer. It has been shown that the piecewise linear function gives simpler expressions for the potential losses due to electron conduction and proton migration without any penalty in the accuracy of the cathode potential. The current density is estimated though lumping the rate of oxygen reduction at the reaction center. Stefan–Maxwell multi-component diffusion equations are employed for the description of mass transport of gaseous species within the diffuser. Investigations on the accuracy of the present performance equations have been carried out for a wide range of parameter values. Computational results reveal that the proposed equations are capable of providing accurate predications for an extended operation domain, namely, from a point near the equilibrium potential to the condition where a limiting current occurs.

Acknowledgements

Financial support from Energy Commission, Ministry of Economic Affairs, Republic of China (contract 92-D0122) is gratefully acknowledged.

References

[1] T. Berning, D.M. Lu, N. Djilali, J. Power Sources 106 (2002) 284.
[2] T.-C. Jen, T.Z. Yan, S.H. Chan, in: Proceedings of the 36th National Heat Transfer Conference, New Orleans, LA, 2002, pp. 1–13.
[3] L. You, H. Liu, Int. J. Heat Mass Transfer 45 (2002) 2277.
[4] S. Um, C.-Y. Wang, K.S. Chen, J. Electrochem. Soc. 147 (2000) 4485.
[5] V. Gurau, H. Liu, S. Kakac, AIChE J. 44 (1998) 2410.
[6] T.F. Fuller, J. Newman, J. Electrochem. Soc. 140 (1993) 1218.
[7] D. Natarajan, T.V. Nguyen, J. Electrochem. Soc. 148 (2001) A1324.
[8] A.A. Kulikovsky, J. Divisek, A.A. Kornyshev, J. Electrochem. Soc. 146 (1999) 3981.
[9] A.C. West, T.F. Fuller, J. Appl. Electrochem. 26 (1996) 557.
[10] W. He, J.S. Yi, T.V. Nguyen, AIChE J. 46 (2000) 2053.
[11] M. Eikerling, A.A. Kronyshev, J. Electroanal. Chem. 453 (1998) 89.
[12] G. Murgia, L. Pisani, M. Valentini, B. D'Aguanno, J. Electrochem. Soc. 149 (2002) A31.

[13] D.M. Bernardi, M. Verbrugge, AIChE J. 37 (1991) 1151.
[14] D.M. Bernardi, M. Verbrugge, J. Electrochem. Soc. 139 (1992) 2477.
[15] C. Marr, X. Li, J. Power Sources 77 (1999) 17.
[16] A. Rowe, X. Li, J. Power Sources 102 (2001) 82.
[17] T.E. Springer, M.S. Wilson, S. Gottesfeld, J. Electrochem. Soc. 140 (1993) 3513.
[18] T.E. Springer, T.A. Zawodzinski, S. Gottesfeld, J. Electrochem. Soc. 138 (1991) 2334.
[19] J. Kim, S.-M. Lee, S. Srinivasan, C.E. Chamberlin, J. Electrochem. Soc. 142 (1995) 2670.
[20] G. Squadrito, G. Maggio, E. Passalacqua, F. Lufrano, A. Patti, J. Appl. Electrochem. 29 (1999) 1449.
[21] J.H. Lee, T.R. Lalk, A.J. Appleby, J. Power Sources 70 (1998) 258.
[22] J.C. Amphlett, R.M. Baumert, R.F. Mann, B.A. Peppley, P.R. Roberge, T.J. Harris, J. Electrochem. Soc. 142 (1995) 1.
[23] J.C. Amphlett, R.M. Baumert, R.F. Mann, B.A. Peppley, P.R. Roberge, T.J. Harris, J. Electrochem. Soc. 142 (1995) 9.
[24] R.F. Mann, J.C. Amphlett, M. Hooper, H.M. Jensen, B.A. Peppley, P.R. Roberge, J. Power Sources 86 (2000) 173.
[25] L. Pisani, G. Murgia, M. Valentini, B. D'Aguanno, J. Power Sources 108 (2002) 192.
[26] C. de Boor, A Practical Guide to Splines, Springer-Verlag, New York, 1978.